IOSR Journal Of Applied Physics (IOSR-JAP)
e-ISSN: 2278-4861.Volume 17, Issue 6 Ser. 1 (Nov – Dec 2025), PP 45-51
www.Iosrjournals.Org

Effect Of Cr^{3+}Ions Substitution On Structural Morphology Of Co-Ferrite Nanoparticles

Suchita V. Deshmukh, Ramesh T. Ubale, Vitthal V. Gaikwad, Atul. P. Keche, Mahesh K. Babrekar, Chandrashekhar M. Kale

Department Of Physics, Indraraj Art, Commerce, And Science College, Sillod. Dist. Chhatrapati Sambhajinagar-431112
Department Of Physics, Siddharth Art, Commerce, And Science College, Jafrabad. Dist. Jalna
Department Of Physics, Moreshwar Art, Commerce, And Science College, Bhokardan. Dist. Jalna
Department Of Physics, R. B. Attal College, Georai. Dist. Beed.

Abstract
A series of polycrystalline nano-ferrite having the chemical formula $CuCr_xFe_{2-x}O_4$(x=0.0, 0.2, 0.4, 0.6, 0.8, and 1.0) were synthesized by sol-gel auto combustion method. X-ray diffraction (XRD) analysis was used to investigate the structural parameters and also to check the phase purity of all prepared samples. The analysis of XRD patterns revealed the formation of single-phase cubic spinel structure for all samples. The average particle size of the synthesized ferrites was identified by X-ray diffraction and scanning electron microscopy technique. Such materials are useful to reduce the energy loss in AC electrical appliances.
Keywords: *Nano-ferrite, particle size, scanning electron microscopy*

Date of Submission: 05-12-2025 Date of Acceptance: 15-12-2025

I. Introduction

In the 21st century, magnetic materials play very important role in the development of nanotechnology. Ferrites are the important magnetic components used in the latest electronic products, such as cell phone, computers, video cameras, memory devices etc. They require small dimensions and all light weights and have better functions. The soft ferrites exhibit two anti-Ferro magnetically coupled sub-lattices namely tetrahedral (A) and octahedral [B] site [1, 2]. The polycrystalline ferrite has very good dielectric properties that are dependent on several factors, such as method of preparation and substitution of different ions. The usefulness of ferrites is influenced by the physical and chemical properties of the materials. The physical properties of polycrystalline ferrites are very sensitive to the micro-structure. The bulk (grain) and grain boundary are the two main components that determine the micro-structure.

Soft ferrites remain of great interest because of their high initial permeability over a large frequency range leading to wide spread applications e.g. inductor cores in RF system, recording heads and microwave devices. Soft ferrites are commercially important materials because of their excellent magnetic and electrical properties [3]. The frustrated magnetic structure in ferrite with the spinel structure can arise when there is a replacement of magnetic ions by non-magnetic ones [4, 5]. The frustration is necessary condition for the appearance of a canted local state, which was first obtained by Rossnewaig [6]. Ferrite (MFe_2O_4, M=Co^{2+}, Ni^{2+}, Fe^{2+}, Zn^{2+}, Cu^{2+} etc.) nanocrystals attract great research interest due to their potential applications in Ferro fluids [7-9], magnetic fluids [10], magnetic recording media [11], magnetic resonance image [12], a remarkable chemical stability and a mechanical hardness, which make it possible material for high density recording media [13].The aim of the present investigations is to study systematically the structural and magnetic properties of chromium substituted copper ferrite prepared by sol-gel auto combustion method.

II. Experimental Details

Material and sample preparation

A series of polycrystalline nanostructured ferrite having the chemical formula $CuCr_xFe_{2-x}O_4$ (x = 0.0, 0.2, 0.4, 0.6, 0.8, and 1.0) were synthesized by using self-propagating sol gel auto combustion method. The starting materials i.e. copper nitrate [Cu $(NO_3)_2 \cdot 6H_2O$], ferric nitrate [Fe $(NO_3)_2 \cdot 9H_2O$], chromium nitrate [Cr $(NO_3)_2 \cdot 9H_2O$], citric acid ($C_6H_8O_7 \cdot H_2O$) and ammonia (NH_3) solution having high purity (99 %, S. D. fine, India) were taken for the preparation of samples. Calculated quantities of metal nitrates were dissolved together in a 100ml of distilled water to get clear solution. An aqueous solution of citric acid was then added to the metal nitrate solution. The molar ratio of citric acid to the total moles of nitrate ions was adjusted to 1:3. A small

amount of NH_3 was added drop wise into the solution so as to adjust pH value nearly equal to 7 so that the sample becomes neutral. A continuous stirring and heating at 90^0C to solution on hot plate with magnetic stirrer until it becomes a very viscous gel. Deionized distilled water was used throughout the complete experimental work. The powder was annealed in air at temperature 500°C for six hours with heating rate 50^0C per min to obtain a spinel phase. The final product is then grinded and were further used without further purification.

Characterization

The X-ray powder diffraction patterns were recorded on Philips X-ray diffractometer wavelength 1.5418 Å. The XRD patterns were recorded in the 2θ range from 20^0 to 80^0 with slow scanning rate 1^0/min. All the structural parameters were calculated from the X-ray diffraction analysis and scanning electron microscopy (SEM). The FTIR spectra in the wave number range 4000- 500 cm^{-1} were recorded at room temperature on spectrometer. Obtained FTIR spectra are used to determine absorption band positions and also analyzed to get structural information about the prepared ferrite systems.

III. Results And Discussion

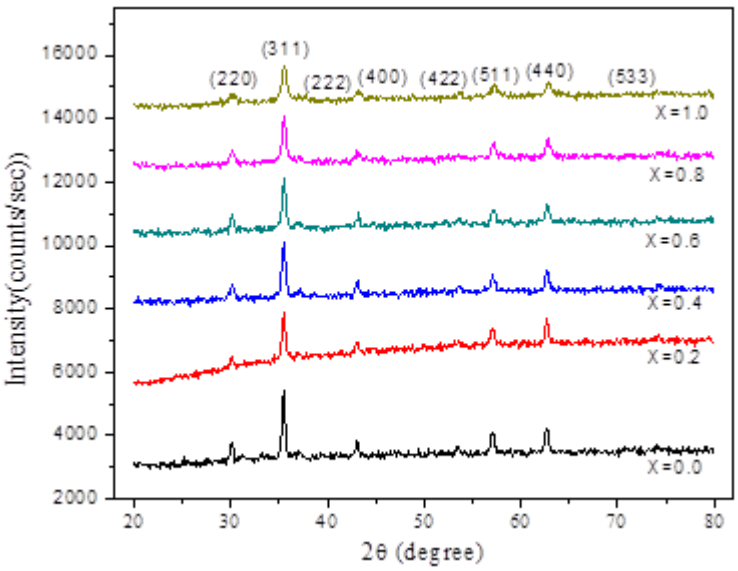

Fig.2: X-ray diffraction patterns of the $CuCr_xFe_{2-x}O_4$ (x = 0.0, 0.2, 0.4, 0.6, 0.8, 1.0) nanoparticles

The X-ray diffraction (XRD) patterns of the $CuCr_xFe_{2-x}O_4$ (x = 0.0, 0.2, 0.4, 0.6, 0.8, 1.0) nano-particles are shown in **Fig.2** for all samples. The entire XRD patterns show the reflections belonging to cubic spinel structure; no extra peaks have been observed in the XRD patterns. The single phase formations of compounds under investigations were confirmed from the analysis of XRD pattern. It is seen that the inter planer spacing (d) values show gradual decrease with increasing Bragg's angle for all the samples. The intensity of (311) plane is more as compared to other planes like (220), (222), (400), (422), (511) and (440) and is chosen for the determination of crystallite size.

Lattice constant (a)

Using XRD data, the lattice parameter has been determined using the method of least squares fitting to an accuracy of ± 0.002 Å and the obtained values of the lattice constant are presented in **Table 1** and the variation of lattice parameter with increase in chromium content 'x' is shown in **Fig.3**. It can be seen from Table 1 and **Fig.3**, that the lattice parameter decreases with increase in Cr^{3+} concentration x. The observed behavior of lattice constant can be explained on the basis of the relative sizes of ionic radii. The ionic radius of Cr^{3+} (0.63Å) ion is smaller than the ionic radius of Fe^{3+} (0.64 Å) ion. Replacement of larger Fe^{3+} cations by smaller Cr^{3+} cations in the copper ferrite causes decrease in lattice parameter. Similar variation of lattice parameter was observed for other Cr^{3+} substituted spinel ferrites [14, 15]. The volume of unit cell (a^3) obtained from lattice parameter (Table 1) values shows decreasing trend with increase in chromium content x. The decrease in volume means the shrinkage of unit cell may be attributed to the substitution of smaller size Cr^{3+} ions in place of larger size Fe^{3+} ions. In the inset of **Fig.3,** the volume of the unit cell shows same nature of lattice constant.

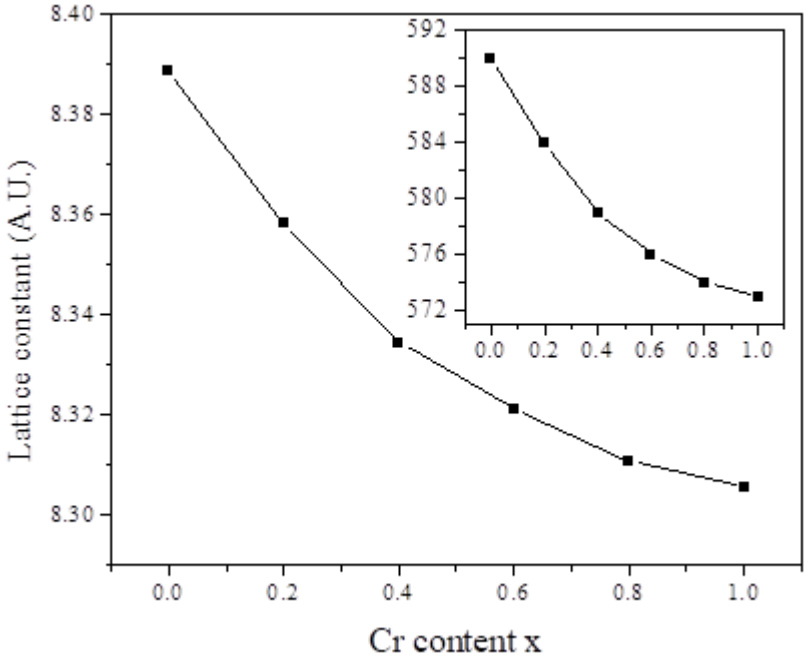

Fig. 3: Lattice constant and volume of the unit cell of the $CuCr_xFe_{2-x}O_4$ (x = 0.0, 0.2, 0.4, 0.6, 0.8, 1.0) nanoparticles

Hopping length (L_A and L_B)

Hopping lengths are the distance between magnetic ions at tetrahedral (A) site (L_A) and octahedral [B] site (L_B) in $CuCr_xFe_{2-x}O_4$ spinel ferrite system. The values of hopping lengths are calculated using the equation,

$$L_A = \frac{a\sqrt{3}}{4} \quad \text{Å} \quad \text{and} \quad L_B = \frac{a\sqrt{2}}{4} \quad \text{Å}$$

Where, 'a' is a lattice constant. The values of hopping length L_A and L_B are given in**. Table 1.** It is observed that both L_A and L_B decreases with chromium concentration x. Since the hopping length depends directly with lattice constant and in the present study the lattice constant decreases with chromium concentration x and therefore both L_A and L_B decreases The results were explained on the basis of decrease in lattice constant with increase in Cr content 'x'. The values of L_A are greater than L_B, shows that the distance between magnetic ions at (A) site is greater than that of [B] site.

Table.1: Lattice constant, unit cell volume and hopping length for $CuCr_xFe_{2-x}O_4$ nanoferrite system.

Sample composition	Lattice constant (a) Å	Unit cell volume (a^3) Å^3	Hopping length Å	
			L_A	L_B
$CuCr_{0.0}Fe_{1.8}O_4$	8.3886	590	3.6323	2.9662
$CuCr_{0.2}Fe_{1.8}O_4$	8.3582	584	3.6191	2.9555
$CuCr_{0.4}Fe_{1.6}O_4$	8.3345	579	3.6088	2.9471
$CuCr_{0.6}Fe_{1.4}O_4$	8.3211	576	3.6030	2.9423
$CuCr_{0.8}Fe_{1.2}O_4$	8.3109	574	3.5986	2.9387
$CuCr_{1.0}Fe_{1.0}O_4$	8.3057	573	3.5964	2.9369

Particle size (t)

The most intense peak (311) of the XRD patterns was used to estimate the particle size of the samples. The particle size was determined using the equation,

$$t = \frac{k\lambda}{\beta \cos\theta} \quad \text{Å}$$

Where, λ is the X-ray wavelength (=1.5405Å) of radiation, k is the shape factor with typical value 0.94, β is the line broadening at full width of half maxima (FWHM) of the (311) diffraction peak and θ is the diffraction angle in radian. The values of particle size are given in **Table 2,** indicates that the particle size is of the order of 28.80 nm to 19.90 nm. It is also observed that the particle size decreases with increase in chromium

concentration x. The particle size depends upon FWHM and Bragg's angle 2θ. In the present study due to substitution of chromium ions higher intensity peak (311) shifts towards higher angle thereby decrease in particle size is observed. Similar results of decrease in particle size due to chromium concentration x was reported [16]. The particle size of prepared sample also be calculated by using scanning electron micrographs (SEM).

Scanning electron micrographs (SEM) analysis

Scanning electron micrographs was used to investigate the change of microstructures of the synthesized $CuCr_xFe_{2-x}O_4$ nanoferrite powder samples with Cr content x. The SEM of the recorded for typical sample x=0.6 and x=0.8 are as shown in **Fig.4.** It can be observed from the SEM images that the prepared samples are amorphous and porous in nature. Particle size obtained by SEM linear intersect method is in the nanometer dimension and the values are given in **Table 2.**

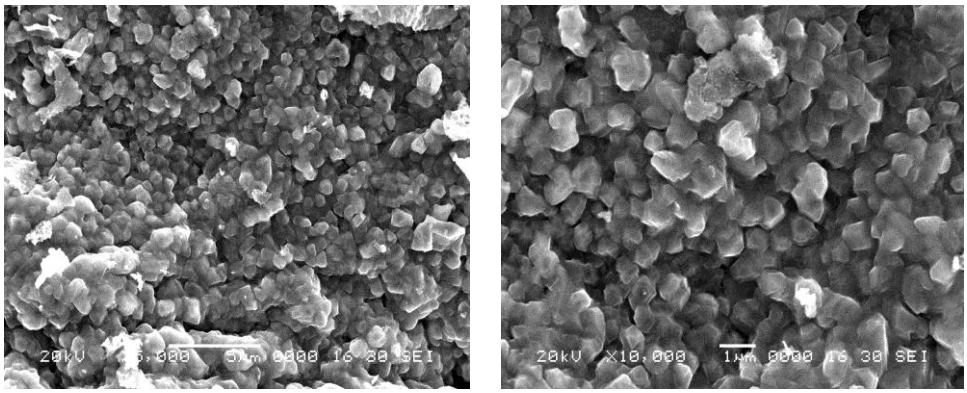

x=0.6 x=0.8

Fig.4: Scanning electron micrograph of $CuCr_xFe_{2-x}O_4$ (where x=0.0 to 1.0) ferrite system with Cr^{3+} ions content x.

In **Fig. 4**, the samples (x=0.6 and x=0.8) show that the particles are agglomerated in irregular shape due to mixed phase and also, observed that the prepared samples are porous in nature indicates that sintering temperature 500^0C is responsible for small amount of pores revels that the sintering is done in a satisfactory manner without loss of Cr^{3+} ions in all samples. The effect of increasing Cr^{3+} ions content on the investigated samples is the enhancement of the grain growth as seen from the SEM. Uniform grains are progressively increased with increasing Cr^{3+} ions content x and the ferrite samples exhibit an aggregated continuous grain growth. The particle size determined from SEM images is in the reported range from 18 to 37 nm which is calculated by linear intercept method [22]**.**

X-ray density (dx)

The X-ray density (dx) was calculated by using the equation,

$$dx = \frac{Z\,M}{Na^3}\ \text{gm/cc}$$

Where, Z is the Number of molecules per unit cell (= 8), M is the Molecular weight of the sample, N is the Avogadro's number, a^3 is the unit cell volume. The X-ray density values are given in Table 2 respectively. The X-ray density decreases with increase in chromium concentration x. The decrease in X-ray density is attributed to the fact that unit cell volume decreases more than the negligible rise in the molar masses of the doped metal cations [17].

Table 2: Particle size, X-ray density, bulk density, % porosity and bond length for $CuCr_xFe_{2-x}O_4$ nano-ferrite system

Cr content x	Particle size (t) nm		X-ray density (dx) gm/cm^3	Bulk density (d_B) gm/cm^3	Percentage porosity (% P)	Bond length Å	
	XRD	SEM				R_A	R_B
0.0	28.80	37	5.510	44.73	44.73	1.903	2.048
0.2	26.58	30	5.480	45.09	45.09	1.896	2.041
0.4	25.68	27	5.470	50.54	50.54	1.891	2.035
0.6	23.56	25	5.460	51.09	51.09	1.888	2.032
0.8	21.43	22	5.470	51.16	51.16	1.886	2.029

1.0	19.90	18	5.460	51.35	51.35	1.884	2.028

Bulk density (d_B)

The bulk density (d_B) was evaluated by using the Archimedes principle. It is observed that bulk density decreases from 3.045 to 2.636 gm/cm^3 with increasing chromium concentration (x = 0.0 to 1.0). The decreasing values of bulk density are given in **Table 2.**

Percentage Porosity (% P)

The percentage porosity (% P) was calculated using the equation,

$$\%\,P = \left(1 - \frac{d_x}{d_B}\right) \times 100$$

Where, d_x is the X-ray density, d_B is the bulk density

The values are tabulated in **Table 2**. The percentage porosity (% P) of the samples increases from 44.43 to 51.35 with increase in Cr^{3+} concentration x of the $CuCr_xFe_{2-x}O_4$ spinel ferrite system [18]. The porosity value shows the effect on particle size of the samples as well as its uses. The high porosity values are useful in coating technology and shielding process.

Bond length (R_A and R_B)

The bond length R_A (is the shortest distance between A site cations and oxygen ion) and R_B (is the shortest distance between B site cations and oxygen ions) for the investigated ferrite system have been calculated and the values of bond lengths R_A and R_B are given in **Table 2**. It is evident from **Table 2** that the bond length R_A and R_B increases with Cr^{3+} ions content x. The decrease in bond length (R_A and R_B) could be attributed to the smaller ionic radius of Cr^{3+} ions than that of Fe^{3+} ions are in good agreement with the reported data [20]

Fourier-transform infrared spectroscopy analysis

Fourier-transform infrared spectroscopy (FTIR) spectroscopic analysis is an additional tool for the structural characterization. In the present investigation the absorption spectra shows two major absorption bands i.e. higher absorption band (υ_1) lies in the range of 567.81 to 605.73 cm^{-1} and lower absorption band (υ_2) in the range 407.02 to 494.61 cm^{-1} are assigned to the tetrahedral (A) and octahedral [B] sites respectively. The values of absorption bands (υ_1 and υ_2) are presented in **Table 3** and shown in **Fig.5** shows that υ_1 and υ_2 goes on increasing with increase in Cr^{3+} ions content.

Table 3: Absorptions band frequency and force constant at (A)-site and at [B]-site, of Cr^{3+} ions content $CuCr_xFe_{2-x}O_4$ nanoferrite system.

Cr content x	Absorptions band frequency (cm^{-1})		Force constant (N/m)	
	ν_1	ν_2	$K_1\times10^5$	$K_2\times10^5$
0.0	567.81	407.02	2.977	1.529
0.2	577.20	412.64	3.076	1.572
0.4	577.73	425.94	3.081	1.675
0.6	582.44	460.49	3.132	1.958
0.8	586.57	492.06	3.176	2.235
1.0	605.73	494.61	3.387	2.259

The difference in frequencies of υ_1 and υ_2 is due to changes in the bond length Fe^{3+}-O^{2-} at tetrahedral and octahedral sites [23]. The remaining bands are probably due to combinational frequencies or overtones. The nature of absorption bands in the FTIR spectra depends on the distribution and type of cations among octahedral and tetrahedral sites [24].

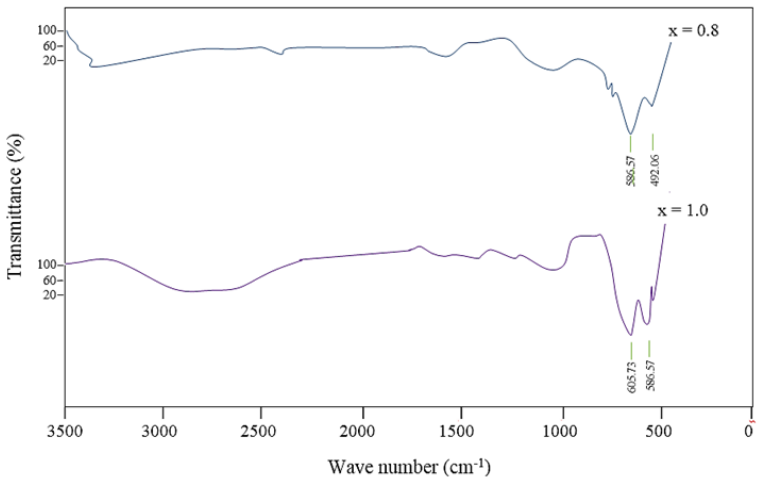

Fig.5: FTIR spectra of Cr^{3+} ions content $CuCr_xFe_{2-x}O_4$ ($0.0 \leq x \leq 1.0$) ferrite system

The force constant for tetrahedral site (K_1) and octahedral site (K_2) was calculated employing the following equation where symbol have their usual meaning,

$K_1 = 7.62 \times M_1 \times \nu_1^2 \times 10^{27}$ (N/m)

$K_2 = 10.62 \times 1.5M_2 \times \nu_2^2 \times 10^{27}$ (N/m)

The values of force constant for tetrahedral site (K_1) and octahedral site (K_2) shown in **Table 3** and represented graphically in **Fig.6.**

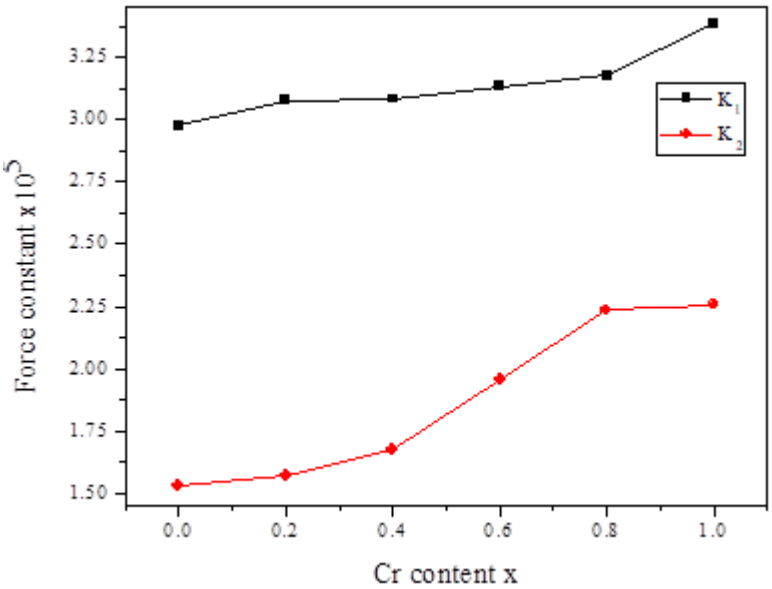

Fig.6. Force constant K_1 and K_2 at (A) and [B] site of Cr^{3+} ions content $CuCr_xFe_{2-x}O_4$ ($0.0 \leq x \leq 1.0$) ferrite system

The force constant of tetrahedral site and octahedral site both are increases as increase in Cr^{3+} ions content x. This behavior can be attributed to the variation in cation oxygen bond length [25]. Since the bond length (A-O) increased with an increase in Cr^{3+} ions content x, the energy required to break longer bonds is less, and this supports a decrease in the force constant of the sites.

IV. Conclusions

After successful investigation of the prepared sample. The conclusions can be drawn from the present study as, prepared sample.

- The chromium substituted copper ferrite system is successfully prepared by sol-gel auto combustion technique. The prepared chromium substituted copper ferrite system shows single phase cubic spinel structure. The lattice constant, volume of the unit cell, hopping length, and structural parameters decreases

with Cr^{3+} ions substitution. Bond length, tetrahedral and octahedral bond edges are directly depends on lattice constant.

- Microstructure studied by SEM technique, shows Nano sized nature of the samples in the reported nanometer range.
- Analysis of room temperature FTIR absorption spectra showed main two absorption bands explains Waldron model used to calculate force constant for both sites.

Reference

[1]. A. Ono, T. Murumo And N. Kaihara: Japan Elec. Eng. 28, 5 (1991)
[2]. T. Normura, And A. Nakano: Proc. Icf6. 1198 (1992)
[3]. J. Smit And H.P.J. Wijn: Ferrites, (Phillips, Technical Laboratory), Holland (1959)
[4]. J. Villain,Z: Phys. B. 33, 31(1979)
[5]. C. P. Poole And H. A. Farach, Z: Phys. B. 47, 55 (1982)
[6]. J. M. Deniels And A. Rossenweig: Can. J. Phys. 48, 381 (1971)
[7]. M. H. Sousa, F. Autorinto, J. Depeyrot, G. J. Da Silve And M. C. Lara: J. Phys. Chem. B. 105, 1168 (2001)
[8]. K. Raj, R. Morkowitz And R. Casciavri: J. Magn. Magn. Mat. 149, 174 (1995)
[9]. T. Hyeon, Y. Chung, J. Park, S. S. Lee, Y. W. Kim And B. H. Park: J.Phys. Chem. B. 6, 6831 (2002)
[10]. R. V. Mehtha, R. V. Upadhyay, B. A. Dasanacharya, P. S. Goyal And K. S. Rao: J. Magn. Magn. Mat. 132, 153 (1994)
[11]. M. H. Kryder: Mat. Res. Soc. Bull. 21, 17 (1996)
[12]. D. G. Mitchell: J. Magn. Reson. Imaging. 7, 1 (1997)
[13]. P. C. Dorsey, P. Lubitz, D. B. Chrisey And J. S. Horowitz: Appl. Phys. 79, 6338 (1996)
[14]. B. L. Shinde, V. S. Suryavanshi And K. S. Lohar: Int. J. Mater. Sci. 12, 3 433-442 (2017)
[15]. S. Imran, N. Amin, M. I. Arshad, M.U. Islam, H. Anwar, A. Azam, M. Ahmad, M. Fakhar- E-Alam, G. Murtaza,G. Mustafa: Digest J. Nanomaterials And Biostructures. 11, 4 1197-1204 (2016)
[16]. Rahul Mundiyaniyil Thankachan, Jincemon Cyriac, B. Raneesh, Nandkumar Kalarikkal, D. Sanyal And P. M. G.Nambisaan: Rsc Advances Issue. 80, (2015)
[17]. Dhole. Et Al.: Ijesrt 5(9), 2016
[18]. M.H.R. Khan, A.K.M. Akther Hossain: J. Magn. Magn. Mater. 324, 550 (2012)
[19]. K. J. Standly: Oxide Magn. Mater. Oxford U. K. Clarendon (1972)
[20]. Zakaria, A.K.M., Nesa, F., Khan, M.S., Yunus, S.M., Khan, N.I., Saha, D.K. And Eriksson, S.G.: J. Bangladesh Academy Sci. 39, (2015)
[21]. R. K. Sharma, V. Sebastian, N. Lakshmi, K. Venugopalan, V. R. Reddy, A. Gupta: Phys. Rev. B. 75, 144419 (2007)
[22]. E. D. Case, J. R. Smyth, And V. Monthei: J. Am. Ceram. Soc. 64, C24-C25, (1981)
[23]. K. A. Mohammeda, A. D. Al-Rawas, A. M. Gismelseed, A. Sellai, .M. Widatallah, A. Yousif , M. E. Elzain , M. Shongwe: Physica B. 407, 795 (2012)
[24]. C. Herzber: Molecular Spectra And Molecular Structure, Van Norstrand Co. Inc., New York (1956)